

Supporting Information

Metal-Oxygen Bonding Characteristics Dictate Activity and Stability Differences of RuO₂ and IrO₂ in Acidic Oxygen Evolution Reaction

Longdan Tang^{1,2}, Xia Chen^{1,2}, Zhuoyang Xie^{1,2}, Qiong Xiang^{1,2}, Jin Liu^{1,2}, Zidong

Wei^{1,2}, Li Li^{1,2*}

¹ State Key Laboratory of Advanced Chemical Power Sources (Chongqing University).

² School of Chemistry and Chemical Engineering, Chongqing University, Chongqing,
400044, China.

*Corresponding author. Email: liliacial@cqu.edu.cn (L. L.)

More DFT computational details

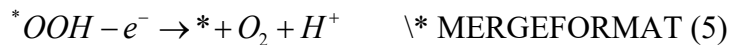
The computational hydrogen electrode(CHE) approach was employed to evaluate OER thermodynamic overpotentials.^{1,2} The Gibbs free energies (G) for the OER were calculated as follows:

$$G = E + ZPE - TS \quad \text{** MERGEFORMAT (1)}$$

where E refers to DFT energy; S and ZPE refer to corrections with entropy through vibrational analysis and zero point energy at 298.15 K, respectively.

Three thermodynamic pathways in our calculations are summarized and the changes in Gibbs free energy (ΔG) of the elementary reactions are calculated as (2–29):

AEM:



$$\Delta G_2 = G_{*OH} + G_{H^+} - G_* - G_{H_2O} - eU \quad \text{** MERGEFORMAT (6)}$$

$$\Delta G_3 = G_{*O} + G_{H^+} - G_{*OH} - eU \quad \text{** MERGEFORMAT (7)}$$

$$\Delta G_4 = G_{*OOH} + G_{H^+} - G_{*O} - G_{H_2O} - eU \quad \text{** MERGEFORMAT}$$

(8)

$$\Delta G_5 = G_* + G_{O_2} + G_{H^+} - G_{*OOH} - eU \quad \text{** MERGEFORMAT (9)}$$

where * denotes the active site of the catalyst; *OH , *O , *OOH are the adsorbed species on the single active site; G_{*OH} , G_{*O} , G_{*OOH} refers to the energy that adsorbs the structure

of *OH, *O, *OOH intermediate; The free energy of H⁺ at standard conditions is assumed as the energy of 1/2 H₂.

LOM:



$$\Delta G_{10} = G_{*_{OH}} + G_{H^+} - G_* - G_{H_2O} - eU \quad \backslash * \text{ MERGEFORMAT (15)}$$

$$\Delta G_{11} = G_{*_{O}} + G_{H^+} - G_{*_{OH}} - eU \quad \backslash * \text{ MERGEFORMAT (16)}$$

$$\Delta G_{12} = G_{O_V} + G_{O_2} - G_{*_{O}} \quad \backslash * \text{ MERGEFORMAT (17)}$$

$$\Delta G_{13} = G_{*_{H_{O-site}}} + G_{H^+} - G_{O_V} - G_{H_2O} - eU \quad \backslash * \text{ MERGEFORMAT (18)}$$

$$\Delta G_{14} = G_* + G_{H^+} - G_{*_{H_{O-site}}} - eU \quad \backslash * \text{ MERGEFORMAT (19)}$$

where Ov denotes lattice oxygen vacancy and *H_{O-site} denotes H adsorbed on the lattice oxygen site, G_{V_O} refers to the energy of the structure with a lattice oxygen vacancy, and $G_{*_{Ho-site}}$ refers to the energy of the structure with H adsorbed on the oxygen site.

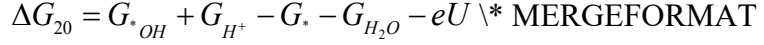
OPM:



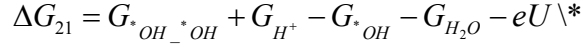
(21)



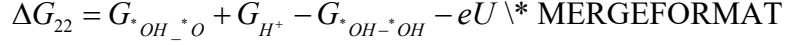
(22)



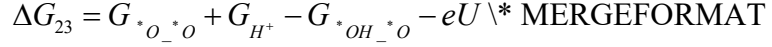
(25)



MERGEFORMAT (26)



(27)



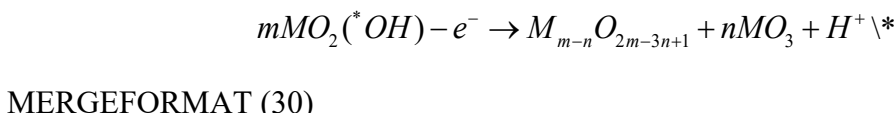
(28)

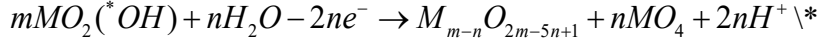


where ${}^*OH_{}^*OH$, ${}^*OH_{}^*O$ and ${}^*O_{}^*O$ represent the adsorbed species on adjacent double active sites, indicating independent adsorption on each site; $G_{*OH_{}^*OH}$, $G_{*OH_{}^*O}$, $G_{*O_{}^*O}$ refer to the energy that adsorbs the structure of ${}^*OH_{}^*OH$, ${}^*OH_{}^*O$ and ${}^*O_{}^*O$ intermediate.

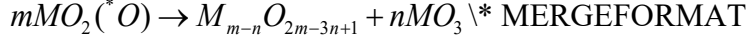
The inactivation mechanism pathways and the calculated dissolution free energy for each step are summarized as follows (30–45):

AEM coupling:





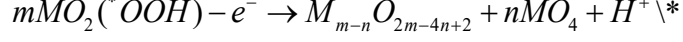
MERGEFORMAT (31)



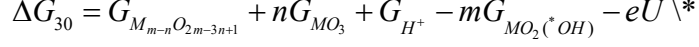
(32)



MERGEFORMAT (33)



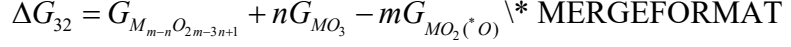
MERGEFORMAT (34)



MERGEFORMAT (35)



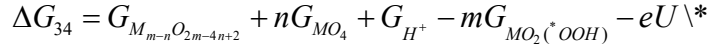
MERGEFORMAT (36)



(37)

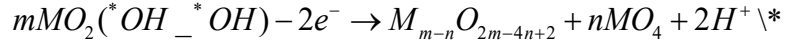


MERGEFORMAT (38)

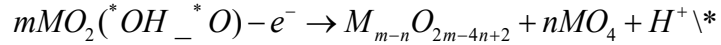


MERGEFORMAT (39)

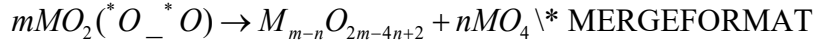
OPM coupling:



MERGEFORMAT (40)



MERGEFORMAT (41)



(42)

$$\Delta G_{40} = G_{M_{m-n}O_{2m-4n+2}} + nG_{MO_4} + 2G_{H^+} - mG_{MO_2(OH)_n} - 2eU \quad \text{\text{*}}$$

MERGEFORMAT (43)

$$\Delta G_{41} = G_{M_{m-n}O_{2m-4n+2}} + nG_{MO_4} + G_{H^+} - mG_{MO_2(OH)_n} - eU \quad \text{\text{*}}$$

MERGEFORMAT (44)

$$\Delta G_{42} = G_{M_{m-n}O_{2m-4n+2}} + nG_{MO_4} - mG_{MO_2(OH)_n} \quad \text{\text{*}} \quad \text{MERGEFORMAT}$$

(45)

where M stands for metal (Ru, Ir); MxOy stands for various models with defect sites; m and n represent the number of initial reaction species and eluted species respectively.

According to reference,^{3,4} the calculation of oxygen vacancy formation energy (ΔG_{V_O}) is as follows:

$$\Delta G_{V_O} = G_{V_O} - G_* + G_O \quad \text{\text{*}} \quad \text{MERGEFORMAT (46)}$$

where G_O is assumed as the energy of 1/2 O₂.

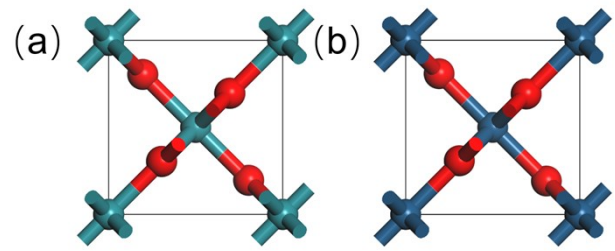


Fig. S1. Optimized geometric structure of the cell model (a) RuO_2 and (b) IrO_2 . (Dark green: Ru; dark blue: Ir; red: O)

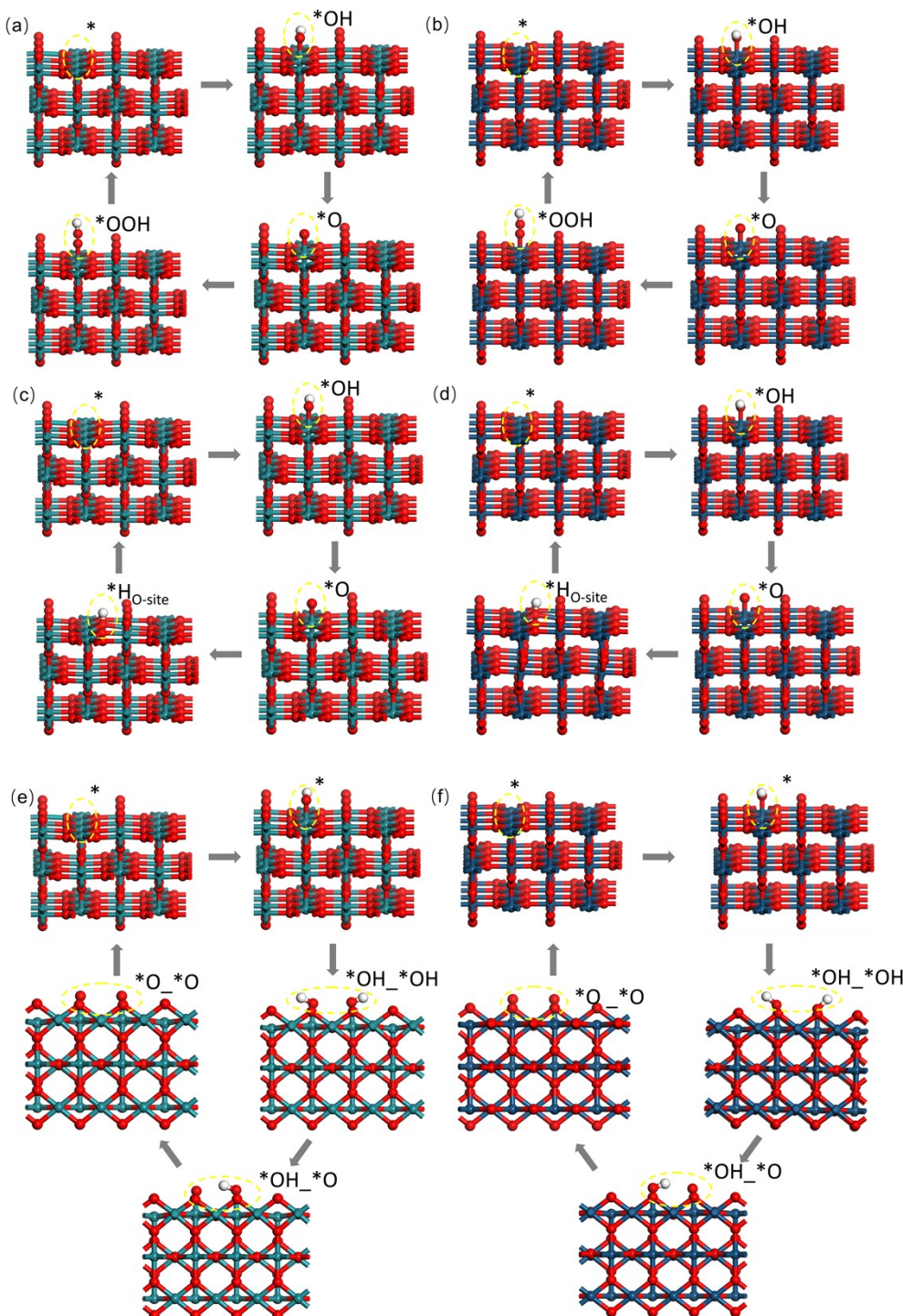


Fig. S2. Structures of the key intermediates in the reaction pathway simulations for complete crystal plane. (a) AEM for RuO₂, (b) AEM for IrO₂, (c) LOM for RuO₂, (d) LOM for IrO₂, (e) OPM for RuO₂, (f) OPM for IrO₂. (Dark green: Ru; dark blue: Ir; red: O; white: H.)



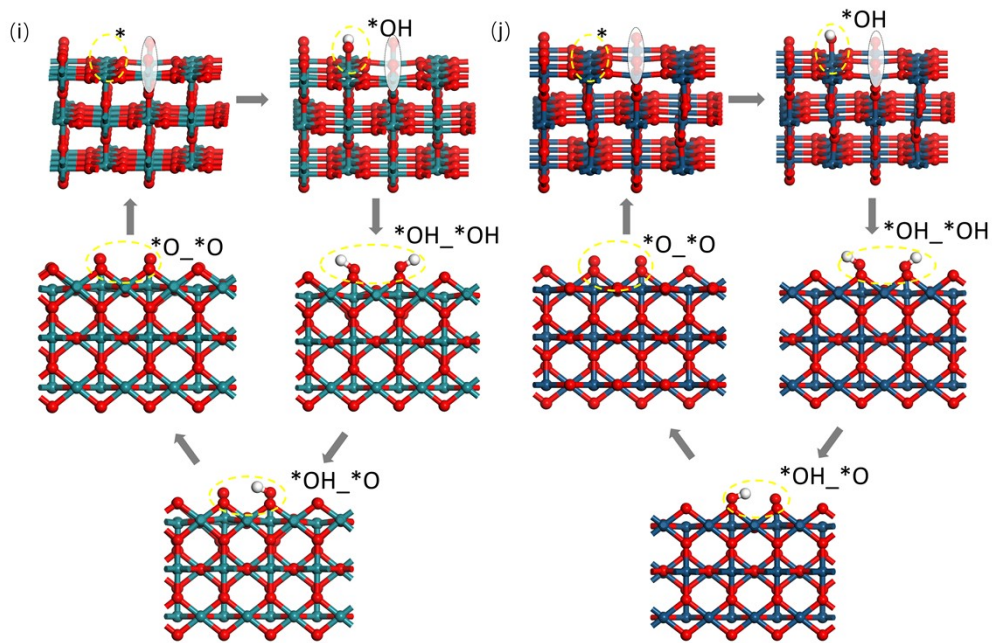


Fig. S3. Structures of the key intermediates for different reaction sites in the reaction pathway simulations on defective crystal plane. (a) AEM on Cus for RuO₂-V, (b) AEM on Cus for IrO₂-V, (c) AEM on Bri for RuO₂-V, (d) AEM on Bri for IrO₂-V, (e) LOM on Cus for RuO₂-V, (f) LOM on Cus for IrO₂-V, (g) LOM on Bri for RuO₂-V, (h) LOM on Bri for IrO₂-V, (h) OPM for RuO₂-V, (i) OPM for IrO₂-V. (Dark green: Ru; dark blue: Ir; red: O; white: H.)

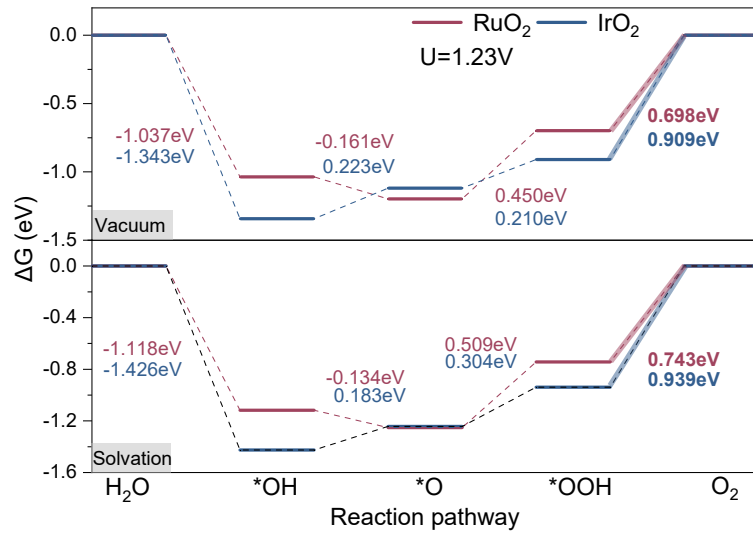


Fig. S4 Gibbs free energy diagrams for OER via AEM at 1.23 V vs. RHE on RuO₂ and IrO₂, comparing vacuum and solvation conditions. Thick lines denote PDS.

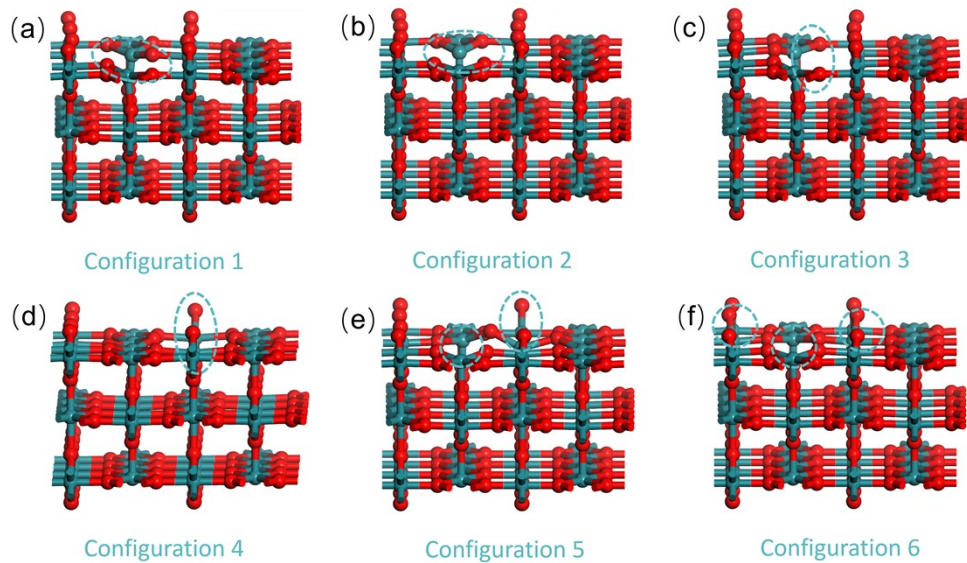


Fig. S5. Six different types of RuxOy configurations from side view. The dotted circles indicate the removal of the metal and oxygen atoms.

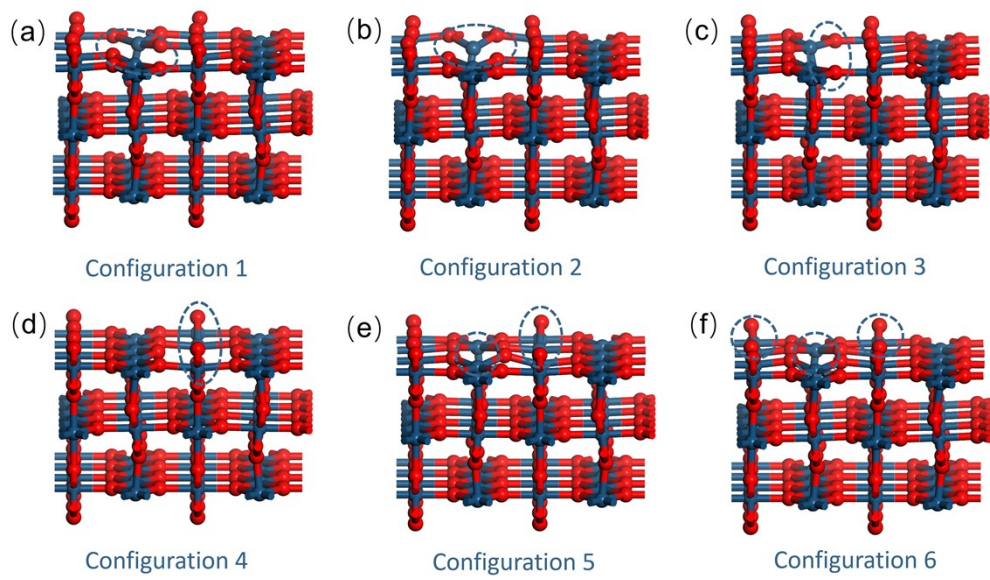


Fig. S6. Six different types of Ir_xO_y configurations from side view. The dotted circles indicate the removal of the metal and oxygen atoms.

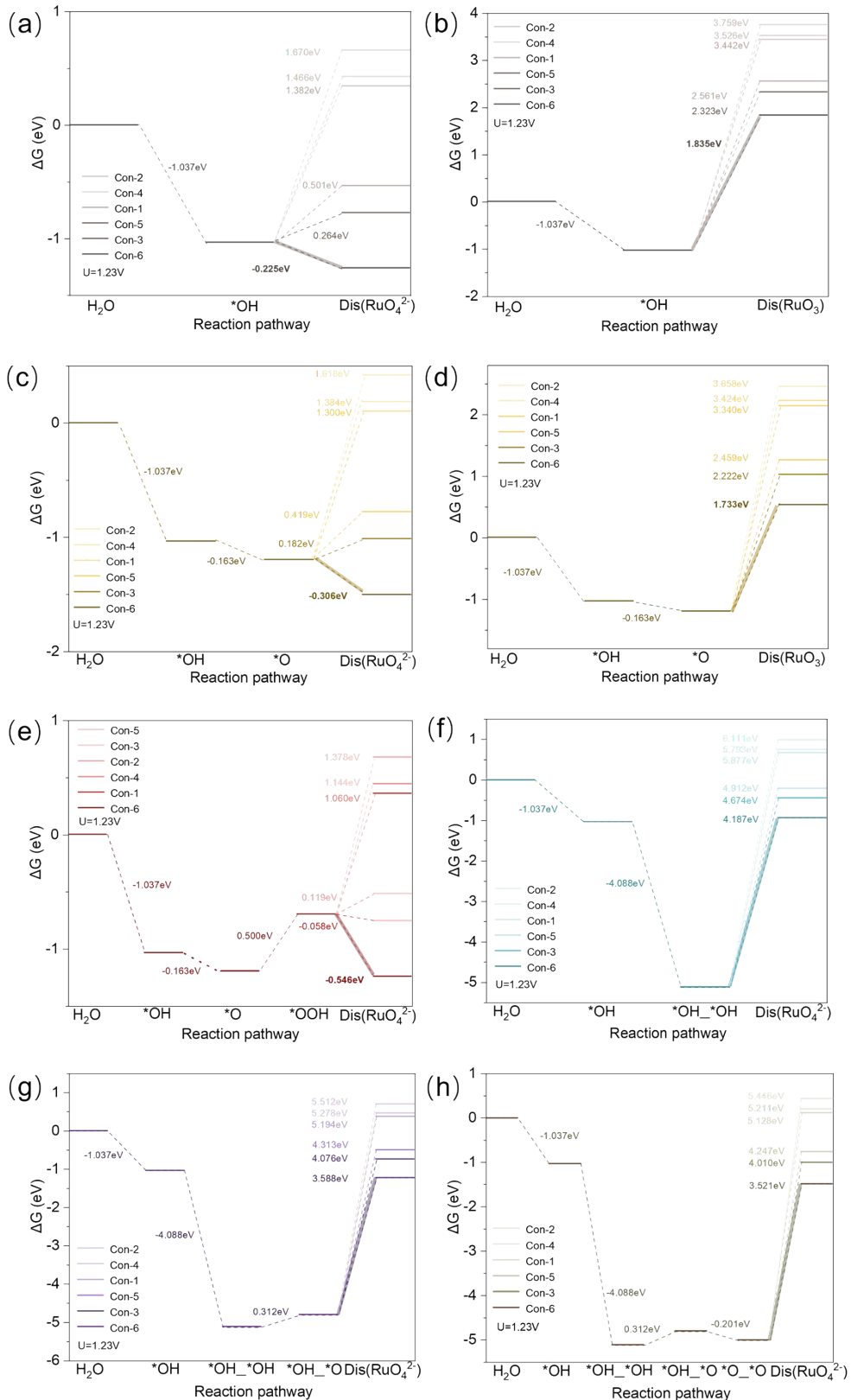


Fig. S7. Dissolution free energy diagram of (a), (b), (c), (d) and (e)AEM, (f)OPM coupling with corrosion for $\text{RuO}_2(110)$ at 1.23V . The thick lines in the figures represent the step that requires the lowest energy for dissolution.

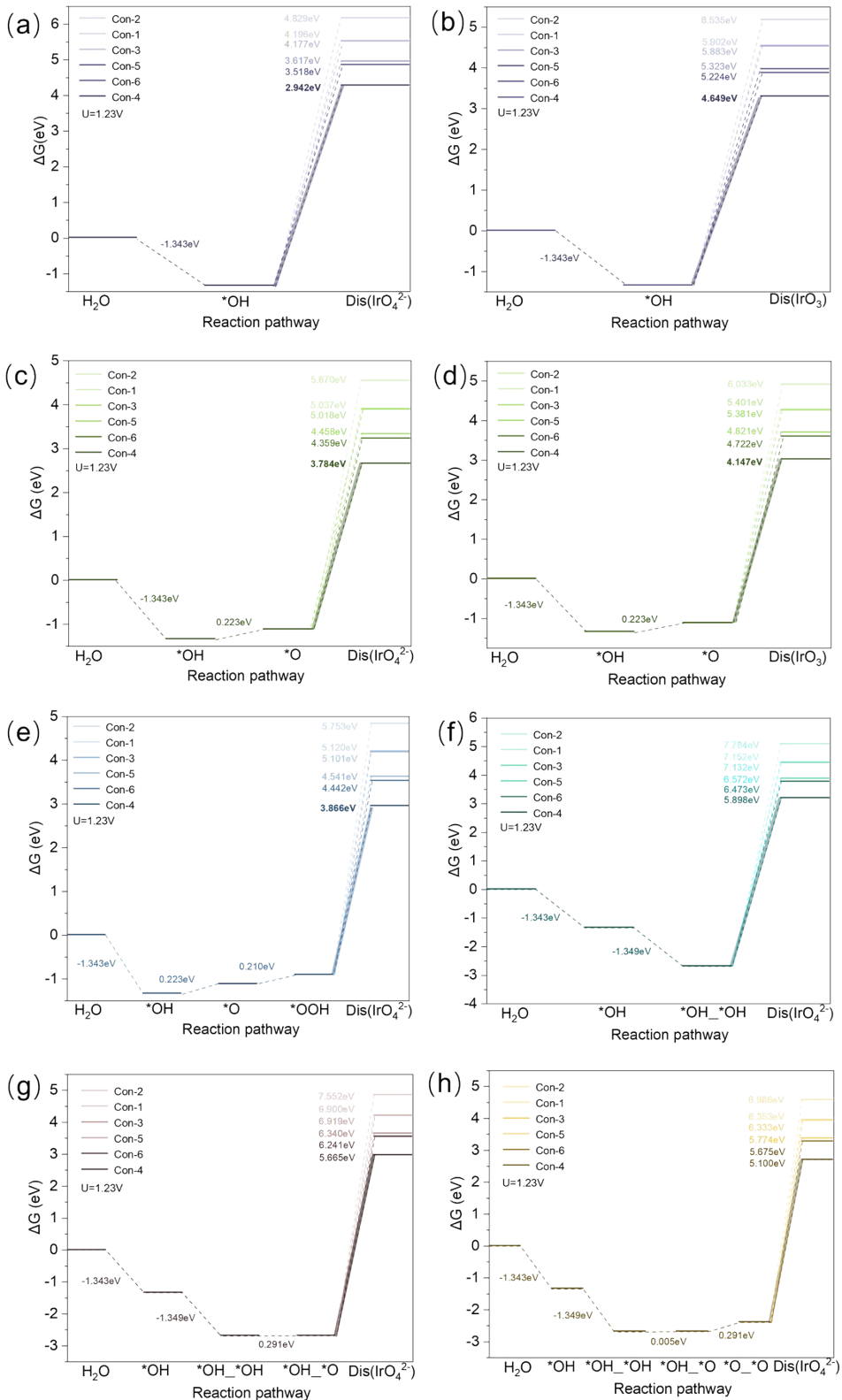


Fig. S8. Dissolution free energy diagram of (a), (b), (c), (d) and (e)AEM, (f)OPM coupling with corrosion for $IrO_2(110)$ at 1.23V. The thick lines in the figures represent the step that requires the lowest energy for dissolution.

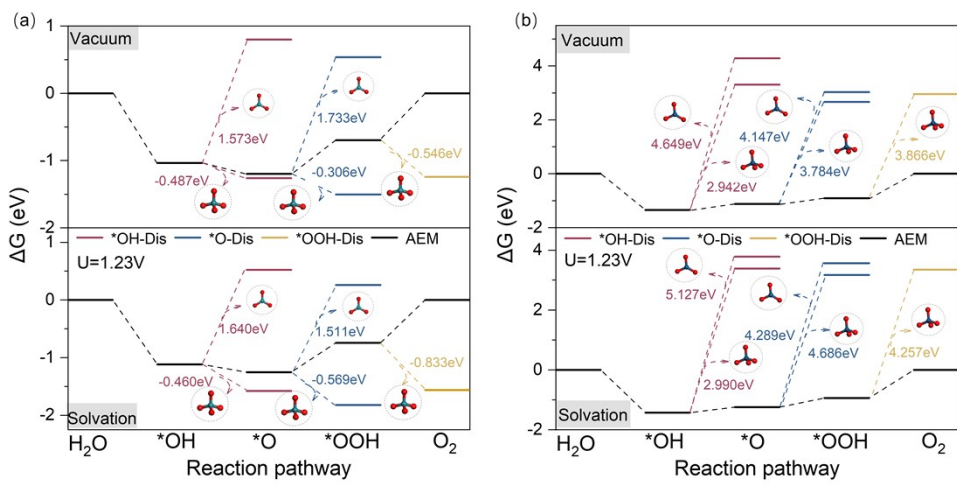


Fig.S9. Comparison of dissolution-free energy diagrams for AEM coupled with corrosion processes of (a) RuO₂ and (b) IrO₂ under both vacuum and solvation conditions at 1.23 V vs. RHE.

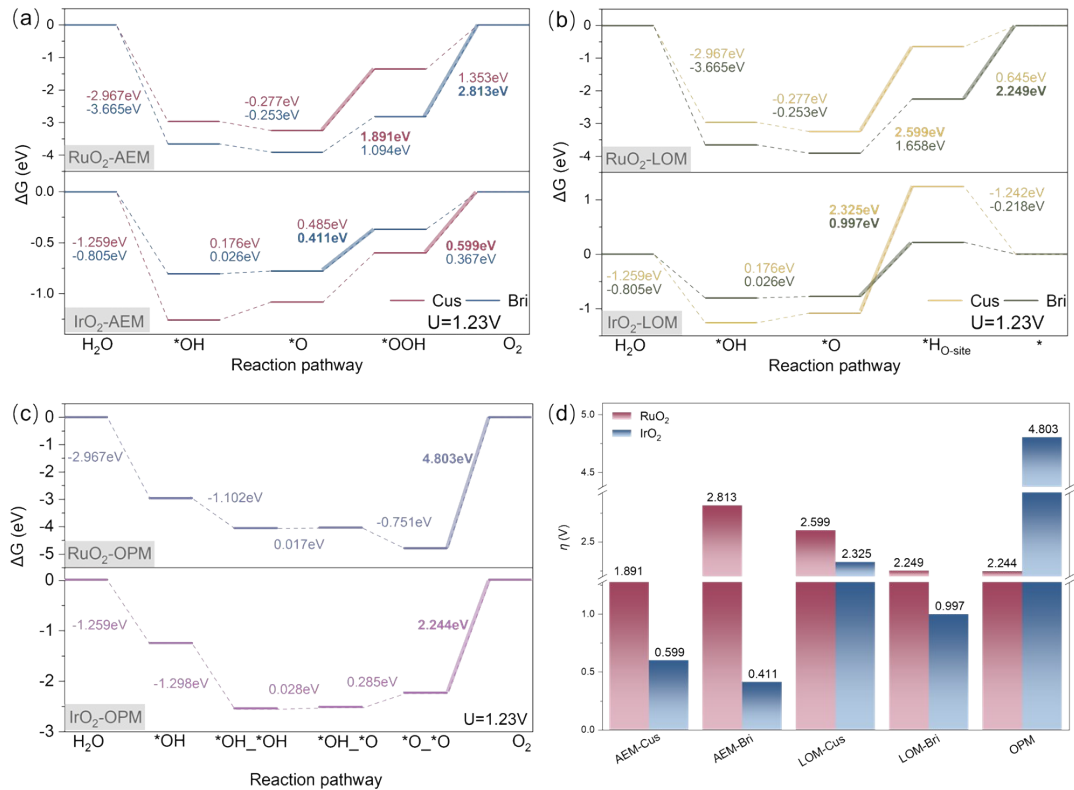


Fig. S10. Gibbs free energy diagrams of (a) and (b)AEM, (c) and (d)LOM, (e)OPM for OER 1.23V on different sites of defective RuO₂ and IrO₂. The thick lines in the figures represent PDS. (d) Overpotential for different reaction pathways for defective RuO₂ and IrO₂.

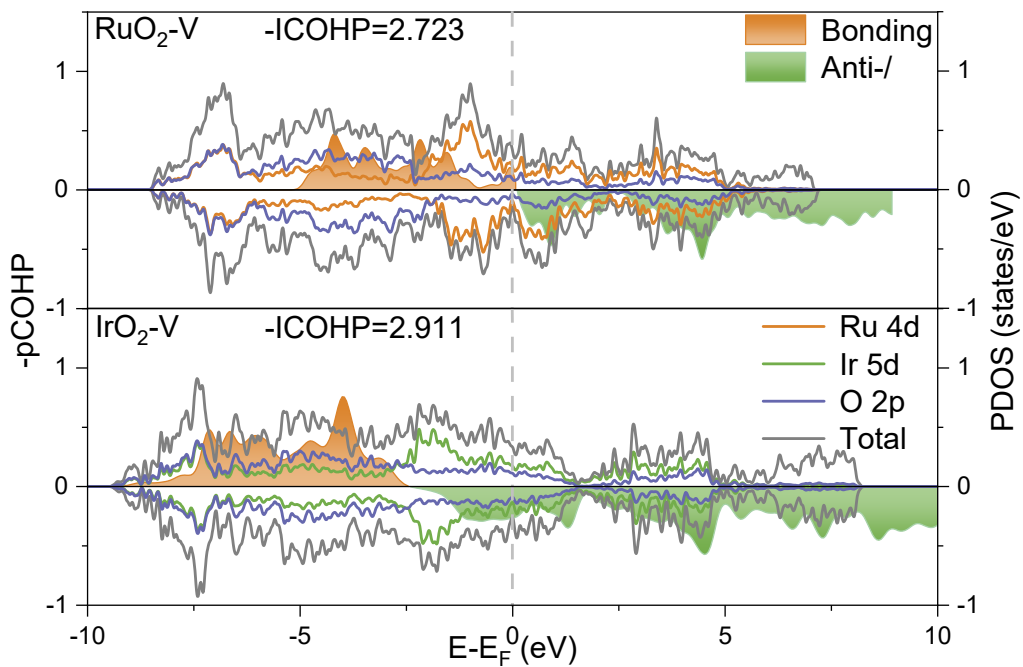


Fig. S11. Projected crystal orbital Hamilton overlap population (pCOHP) curves and projected density of states (PDOS) plots of M-d and O-p in the RuO₂-V and IrO₂-V models. The dashed line refers to the Fermi level.

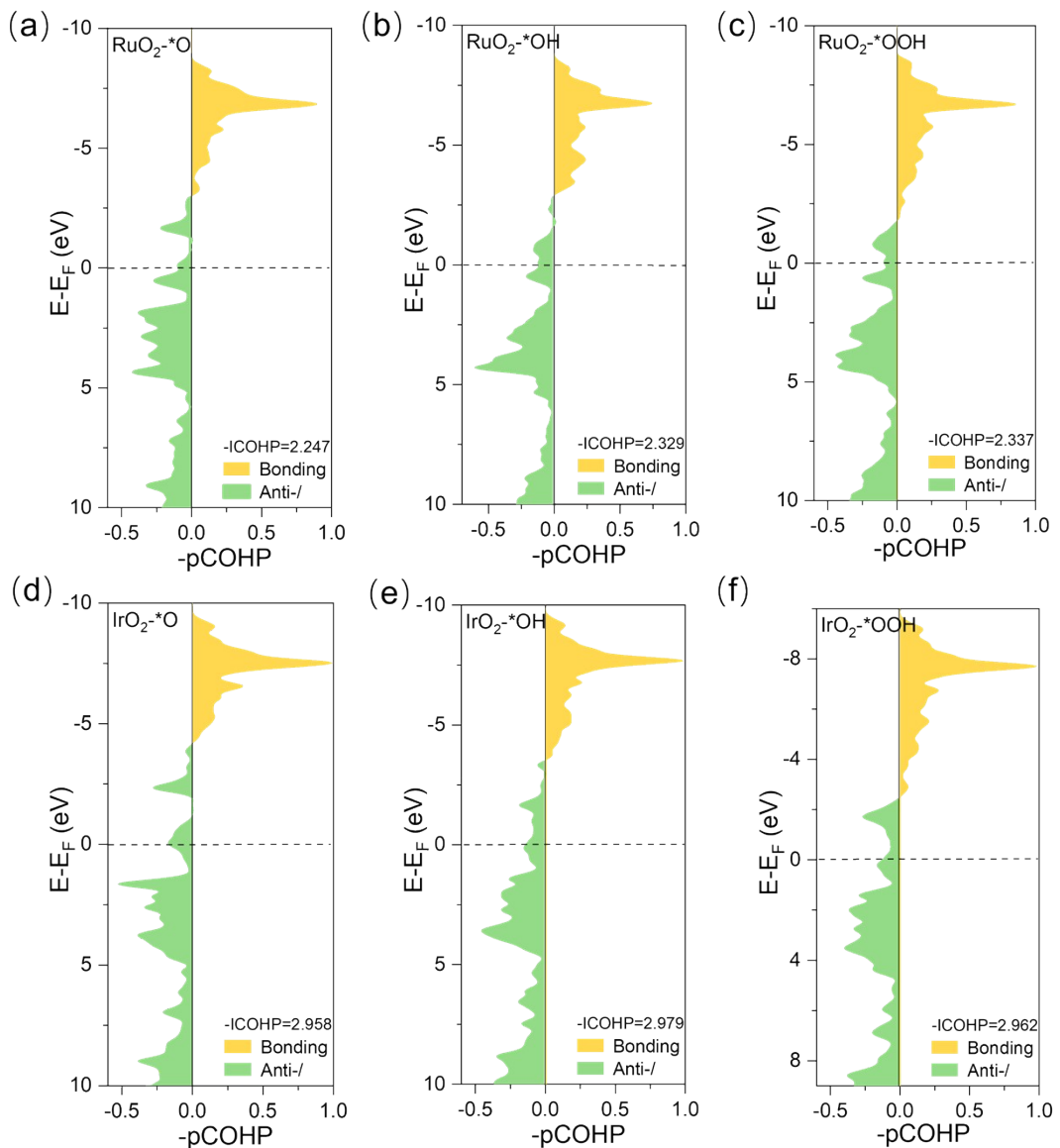


Fig. S12. Projected crystal orbital Hamilton overlap population (pCOHP) curves in the bulk RuO_2 and IrO_2 models after the adsorption of different intermediates. (a) RuO_2 adsorbed $^*\text{O}$, (b) RuO_2 adsorbed $^*\text{OH}$, (c) RuO_2 adsorbed $^*\text{OOH}$, (d) IrO_2 adsorbed $^*\text{O}$, (e) IrO_2 adsorbed $^*\text{OH}$ (f) IrO_2 adsorbed $^*\text{OOH}$.

Table S1. Lattice parameters of the modeled structures after optimization.

Modeled structures	Lattice parameters					
	a(Å)	b(Å)	c(Å)	α(°)	β(°)	γ(°)
RuO ₂ (cell)	4.490	4.490	3.118	90	90	90
IrO ₂ (cell)	4.527	4.527	3.173	90	90	90
RuO ₂ (110)	12.472	12.697	29.523	90	90	90
IrO ₂ (110)	12.692	12.806	28.860	90	90	90

Table S2. Bond length (Å) and bond angle (°) parameters of the modeled structures after optimization.

Modeled	M _{cus} -O _{cus}	M _{bri} -O _{bri}	M _{bri} -O _{cus}	O-M-O(cus)	O-M-O(bri)
RuO ₂ (cell)	1.994	1.994	1.930	102.836	102.836
IrO ₂ (cell)	2.007	2.007	1.973	104.493	104.493
RuO ₂ (110)	1.981	1.910	1.968	75.215	109.431
IrO ₂ (110)	2.008	1.979	1.976	75.233	106.598

Table S3. The calculation of oxygen vacancy formation energy (ΔG_{V_o}).

Surface	ΔG_{V_o} , eV	
	This work	Ref
RuO ₂ (110)	3.169	1.67 ⁵
IrO ₂ (110)	3.441	2.04 ⁶

Table S4. The calculation of co-defect formation energies for metals and oxygen (ΔG_V).

Modeled structures	ΔG_V , eV	
	RuO ₂ (110)	IrO ₂ (110)
Configuration 1	6.457	9.032
Configuration 2	6.773	9.665
Configuration 3	5.337	9.012
Configuration 4	6.539	7.778
Configuration 5	5.574	8.452
Configuration 6	4.848	8.354

Table S5. The calculation of $\epsilon_d - \epsilon_p$, ELF and -ICOHP.

Modeled structures	$\epsilon_d - \epsilon_p$, eV	ELF	-ICOHP
RuO ₂ (110)	1.328	0.475	2.412
IrO ₂ (110)	1.456	0.511	2.942
RuO ₂ -V	1.493		2.723
IrO ₂ -V	1.317		2.911

REFERENCES

- 1 J. K. Nørskov, J. Rossmeisl, A. Logadottir, L. Lindqvist, J. R. Kitchin, T. Bligaard and H. Jónsson, Origin of the Overpotential for Oxygen Reduction at a Fuel-Cell Cathode, *J. Phys. Chem. B*, 2004, **108**, 17886–17892.
- 2 I. C. Man, H. Su, F. Calle-Vallejo, H. A. Hansen, J. I. Martínez, N. G. Inoglu, J. Kitchin, T. F. Jaramillo, J. K. Nørskov and J. Rossmeisl, Universality in Oxygen Evolution Electrocatalysis on Oxide Surfaces, *ChemCatChem*, 2011, **3**, 1159–1165.
- 3 M. G. Kim and Y.-H. Choi, Electrocatalytic Properties of Co₃O₄ Prepared on Carbon Fibers by Thermal Metal–Organic Deposition for the Oxygen Evolution Reaction in Alkaline Water Electrolysis, *Nanomaterials*, 2023, **13**, 1021.
- 4 C.-Z. Yuan, S. Wang, K. San Hui, K. Wang, J. Li, H. Gao, C. Zha, X. Zhang, D. A. Dinh, X.-L. Wu, Z. Tang, J. Wan, Z. Shao and K. N. Hui, In Situ Immobilizing Atomically Dispersed Ru on Oxygen-Defective Co₃O₄ for Efficient Oxygen Evolution, *ACS Catal.*, 2023, **13**, 2462–2471.
- 5 Z.-Y. Wu, F.-Y. Chen, B. Li, S.-W. Yu, Y. Z. Finfrock, D. M. Meira, Q.-Q. Yan, P. Zhu, M.-X. Chen, T.-W. Song, Z. Yin, H.-W. Liang, S. Zhang, G. Wang and H. Wang, Non-iridium-based electrocatalyst for durable acidic oxygen evolution reaction in proton exchange membrane water electrolysis, *Nat. Mater.*, 2023, **22**, 100–108.
- 6 A. Zagalskaya and V. Alexandrov, Role of Defects in the Interplay between Adsorbate Evolving and Lattice Oxygen Mechanisms of the Oxygen Evolution Reaction in RuO₂ and IrO₂, *ACS Catal.*, 2020, **10**, 3650–3657.